Geometric Relation Distribution for Place Recognition

Dario Lodi Rizzini[1,2], Francesco Galasso[1] and Stefano Caselli[1,2]

***Abstract*—In this paper, we illustrate Geometric Relation Distribution (GRD), a novel signature for place recognition and loop closure with landmark maps. GRD encodes geometric pairwise relations between landmark points into a continuous probability density function. The pairwise angles are represented by von Mises distribution whereas two alternative distributions, Erlang or biased Rayleigh, are proposed for distances. The GRD function is represented through its expansion into Fourier series and Laguerre polynomial basis. Such orthogonal basis representation enables efficient computation of the translation and rotation invariant metric used to compare signatures and find potential loop closure candidates. The effectiveness of the proposed method is assessed through experiments with standard datasets.**

***Index Terms*—Mapping; Localization; Range Sensing**

I. Introduction

An important task in robot localization and mapping is the recognition of already visited regions during navigation. When the recognition takes place after the robot has travelled long paths, this operation is called *loop closure*. Loop closure enables to recover localization errors and map inconsistencies due to cumulative odometry error by estimating the relative transformation between the current robot frame and the matching one. While this problem has been extensively investigated for several sensor and map models like occupancy grid maps from range finders or computer vision keypoint features, robust loop closure techniques for landmark maps have been developed quite recently [1]–[5].

The keypoint features [3], [6] detected in range finder scans naturally constitute local maps of landmarks. The landmark coordinates of each local map are referred to the corresponding local keyframe. Given this formulation, loop closure is achieved by associating a query landmark set and all the stored landmark sets in the global map. Direct landmark-to-landmark association is neither computationally efficient nor reliable over large collections of points. Thus, most loop closure methods perform point-to-point matching, after selection of candidates by comparing *signatures*. Several signatures [1], [5] are designed on bag-of-word (BoW) and explicitly require features with descriptors. BoW approaches rely on descriptors and their performance is affected when descriptors poorly characterize landmark neighborhoods. Signatures like GLARE [2] and GLAROT [4] encode the geometric relations between the features like pairwise distances and relative angles into histograms. In particular, GLAROT is invariant to translation and rotation in order to detect visited submaps regardless of viewpoint. These signatures capture distinctive distribution of feature points and do not require neither specific descriptors nor preliminary dictionary as for BoW approaches. However, their histogram-based representation is sensitive to the resolution of the discretized geometric parameters.

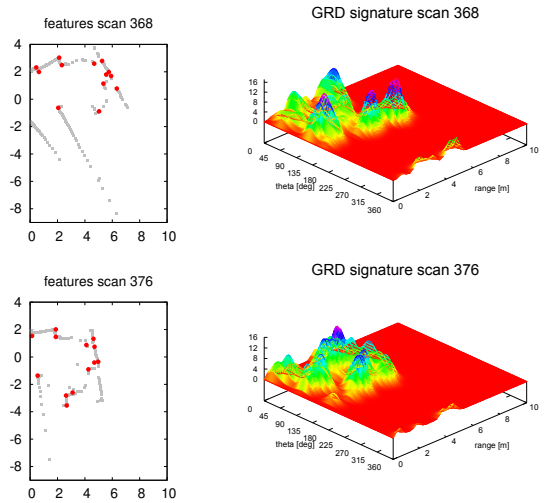

Fig. 1: Examples of GRD signature. Left: the scans 368 and 376 of dataset *intel-lab* (grey) and the SKIP keypoints (red) detected in the respective scan. Right: the corresponding GRD signatures based on biased Rayleigh distribution obtained from each of the two point sets.

In this paper, we propose the novel signature *Geometric Relation Distribution* (GRD) for place recognition and loop closure detection in landmark maps. Like GLARE and GLAROT, GRD encodes geometric relations between landmarks, but its representation corresponds to the probability density function (PDF) of pairwise angles and distances between features. The PDF is multi-modal with a mode for each pair of features. The PDF mode is the product of two marginal distributions, respectively von Mises for angles and Erlang or biased Rayleigh for distances. Moreover, the GRD distribution is expanded into a series of orthogonal functions based on Fourier series

Manuscript received: September 10 2018; Revised: December 4 2018; Accepted December 24 2018.

This paper was recommended for publication by Editor Cyrill Stachniss upon evaluation of the Associate Editor and Reviewers' comments. This work is supported by 3DPAL project, a spin-off of the SIMON project sponsored by Regione Emilia-Romagna, CUP E18I17000110009.

[1]Authors are with RIMLab - Robotics and Intelligent Machines Laboratory, Dipartimento di Ingegneria e Architettura, University of Parma, Italy, {dario.lodirizzini, francesco.galasso, stefano.caselli}@unipr.it.

[2]First and Third Authors are also with Centro Interdipartimentale per l'Energia e l'Ambiente (CIDEA), University of Parma, 43124, Italy.

Digital Object Identifier (DOI): see top of this page.

and Laguerre polynomials. The truncated series can effectively incorporate arbitrary number of modes using the same basis in order to scale with arbitrary number of features. The series is used to efficiently compute a rotation-invariant correlation metric. The performance of GRD has been assessed through experiments with standard benchmark datasets and compared with the state-of-the-art signatures and loop closure detection algorithms.

The paper is organized as follows. Section II reviews the state of the art of loop closure algorithms for landmark maps. Section III illustrates GRD and its efficient representation with orthogonal function basis. Section IV presents a transformation invariant metric. Section V reports the experimental results. Section VI concludes the work.

II. Related Works

The landmark map model is based on the extraction of point features from sensor measurements. Paradoxically, the development of robust keypoint features for planar range finders is quite recent acquisition. Tipaldi et al. [6] proposed FLIRT, the first keypoint feature using multiscale approach and descriptors inspired by computer vision features. FALKO features [3] enable detection of more stable keypoints based on careful neighborhood selection and cornerness score. FALKO keypoints also support descriptors for encoding neighbor point distribution in order to improve data association and, possibly, loop closure.

During mapping, one of the problems arising is place-recognition used for loop closure action, in order to identify already visited poses. Loop candidates must be selected using a robust signature to avoid recognition error. Gutmann et al. [7] proposed Local Registration and Global Correlation (LRGC), an incremental method for reconstruction of global maps from range data. Geometrical FLIRT phrases (GFPs) [1] were proposed as an efficient and reliable place recognition exploiting FLIRT descriptors and the bag-of-words (BoW) approach. Deray et al. [5] improved BoW association using a Viterbi algorithm and weak geometric check achieving better loop closure performance. Geometric LAndmark RElations (GLARE) [2], [8] have been proposed to transform 2D laser scans into pose invariant histogram representations evaluating invariant pairwise distances and angles between scan points. Nevertheless, this approach is not orientation invariant. GLAROT [4] was introduced as an improvement over GLARE and designed to be rotation invariant. Point-to-point data association algorithms like maximum clique methods [9], [10] or joint compatibility test [11] are required to check the selected candidates and to estimate the transformation. A different approach includes the loop closure methods comparing complete scans or local maps with registration algorithms. Lu and Milios [12] proposed the first registration-based loop closure algorithm based on a variant of iterative closest point (ICP). More recent registration methods for loop closure include ICP in pose graphs [13] and efficient alignment of occupancy grid maps [14].

Similar problems are faced when building a map with 3D point clouds. The work in [15] extends GLAROT to space domain through an approximately regular binning of sphere. Tazaki et al. [16] proposed a loop detection method as a pair of partial time series showing high similarity score. Kim et al. [17] introduced a new descriptor for 3D laser scans embedded with an efficient search algorithm based on KD tree online with Ring Key for fast search. Multiple point cloud registration [18] can improve robustness of point-to-point association.

III. Pairwise Point-Signature Distribution

Given a set of 2D points $\mathcal{P}$, the pairwise angles and distances of two different points $\mathbf{p}_i, \mathbf{p}_j \in \mathcal{P}$ (assume that $p_{i,y} > p_{j,y}$) are defined respectively as

$$\hat{\theta}_{ij} = \operatorname{atan2}(p_{i,y} - p_{j,y}, p_{i,x} - p_{j,x}) \qquad \hat{r}_{ij} = \|\mathbf{p}_i - \mathbf{p}_j\| \quad (1)$$

When the input points are acquired through sensors, their coordinates are noisy and uncertain. The point set $\mathcal{P}$ may represent keypoint features extracted from a given robot location. While their Cartesian coordinates are dependent on the viewpoint, their pairwise distances and angles are respectively invariant or invariant up to a rotational offset. Our goal is to define a *signature* using the distribution of pairwise angle θ and distance r on $\mathcal{P}$ disregarding the exact pairs. Each pair (i, j) contributes to each mode $\mathcal{P}_{ij}$ of the global distribution of θ and r. The probability density function (PDF) of $[\theta, r]$ associated to $\mathcal{P}$ is

$$p_{\theta r}(\theta, r) = \sum_{i=1}^{n_p} \sum_{j=i+1}^{n_p} p_{\theta r}(\theta, r|\mathcal{P}_{ij})\ p(\mathcal{P}_{ij}) \quad (2)$$

Hence after, we assume that all the modes are equally likely and $p(\mathcal{P}_{ij}) = 1/N$, where $N = n_p(n_p - 1)/2$. Moreover, we assume that $p_{\theta r}(\theta, r|\mathcal{P}_{ij})$ can be factorized into the product of the independent PDFs of θ and r as

$$p_{\theta r}(\theta, r|\mathcal{P}_{ij}) = p_{\theta_{ij}}(\theta)\ p_{r_{ij}}(r) \quad (3)$$

The two marginal distributions $p_{\theta_{ij}}(\theta)$ and $p_{r_{ij}}(r)$ must be chosen consistently with the random variable domain. The *von Mises distribution* is often used for angular statistics with central mode in preference to the more mathematically cumbersome wrapped normal distribution. Thus, it is used as model for θ with mean values $\hat{\theta}_{ij}$. The probability density function $p_{r_{ij}}(r)$ must represent a random variable on interval $[0, +\infty)$ and single mode in $\hat{r}_{ij}$. There are several models for this purpose and in this work we discuss *Erlang* and *biased Rayleigh* distributions. The PDF $p_{\theta r}(\theta, r)$ in eq. (3) has the form of weighted sum of uni-modal kernels, which is not convenient for efficient algebraic manipulation. Moreover, a metric invariant to rigid transformation is required to compare two different signatures. The rest of this section is devoted to address these problems.

A. Pairwise Angle Statistics with Von Mises distribution

The probability density function of the von Mises distribution is

$$p_{\theta_{ij}}(\theta) = \frac{1}{2\pi \mathrm{I}_0(\kappa)}\ \exp\left(\kappa\ \cos\left(\theta - \hat{\theta}_{ij}\right)\right) \quad (4)$$

This article has been accepted for publication in a future issue of this journal, but has not been fully edited. Content may change prior to final publication. Citation information: DOI 10.1109/LRA.2019.2891432, IEEE Robotics and Automation Letters

where $\mathrm{I}_0(\kappa)$ is the modified Bessel function of order 0, $\hat{\theta}_{ij}$ is the mean value and also the maximum of density of probability, and κ is the so called concentration parameter, a reciprocal measure of dispersion. We assume that the concentration parameter κ is the same for all the angles. The distribution can be expanded into *Fourier series* [19, (9.6.34)] as

$$p_{\theta_{ij}}(\theta) = \frac{1}{2\pi} + \sum_{k_\theta=1}^{+\infty} \left(a_{k_\theta}^{ij} \cos(k_\theta \theta) + b_{k_\theta}^{ij} \sin(k_\theta \theta) \right) \tag{5}$$

$$a_{k_\theta}^{ij} = \frac{\mathrm{I}_{k_\theta}(\kappa) \cos\left(k_\theta \hat{\theta}_{ij}\right)}{\pi \mathrm{I}_0(\kappa)} \quad b_{k_\theta}^{ij} = \frac{\mathrm{I}_{k_\theta}(\kappa) \sin\left(k_\theta \hat{\theta}_{ij}\right)}{\pi \mathrm{I}_0(\kappa)} \tag{6}$$

The infinite Fourier series is usually truncated to term n_θ as $s_{n_\theta}(\theta)$. A bound on the approximation error has been derived in [20] as

$$\left| p_{\theta_{ij}}(\theta) - s_{n_\theta}(\theta) \right| \leqslant \frac{\mathrm{I}_{n_\theta}(\kappa)}{\pi \mathrm{I}_0(\kappa)} \frac{\kappa}{n_\theta} \tag{7}$$

Such bound largely overestimates the error, but can be used to compute the number of terms n_θ needed to guarantee the required maximum error.

B. Erlang distribution for Pairwise Distance

The random variable r representing the pairwise distance between two points is defined on domain $[0, +\infty)$ and has single mode corresponding to the measured one. The Erlang distribution is among the probability distributions which satisfy such conditions. Given the scale parameter $\eta_{ij} > 0$ and shape parameter $d_{ij} \in \mathbb{N}$, the PDF of an Erlang distribution is

$$p_{r_{ij}}(r) = \frac{r^{d_{ij}-1} \, \mathrm{e}^{-\frac{r}{\eta_{ij}}}}{\eta_{ij}^{d_{ij}} \, (d_{ij}-1)!} \tag{8}$$

The Gamma distribution is a generalization of Erlang where parameter d_{ij} can be any positive real number. The mean value $\eta_{ij} d_{ij}$ and variance $\eta_{ij} d_{ij}^2$ of Erlang distribution depend on its two parameters. Since the shape parameter d_{ij} is integer not all the values of mean and variance are simultaneously feasible.

Like in the case of von Mises, Erlang distribution can be represented by a linear combination of orthogonal functions. Since the domain is the positive real line $r \geqslant 0$, the natural basis is given by *Laguerre polynomials* [21]. The Erlang can be expanded in Laguerre polynomial series with coefficients $\{c_{k_r}\}$ as

$$p_{r_{ij}}(r) = \sum_{k_r=0}^{+\infty} c_{k_r}^{ij} \, L_{k_r}(r) \tag{9}$$

where $L_{k_r}(r)$ is the Laguerre polynomial of order k_r. The convergence of Laguerre series to a function is guaranteed, when the function satisfies proper condition [21, sec. 4.23]. This condition is satisfied by all the probability density functions. Such polynomials are orthogonal w.r.t. integral inner product with weight function e^{-r}, i.e.

$$\langle L_i, L_j \rangle_{\mathrm{e}^{-r}} = \int_0^{+\infty} \mathrm{e}^{-r} \, L_i(r) \, L_j(r) \, dr = \delta_{ij} \tag{10}$$

where δ_{ij} is the Kroenecker delta. Hence, the coefficient $c_{k_r}^{ij}$ is given as

$$\begin{aligned} c_{k_r}^{ij} &= \langle p_{r_{ij}}, L_{k_r} \rangle_{\mathrm{e}^{-r}} \qquad (11) \\ &= \sum_{m=0}^{k_r} \binom{k_r}{m} \frac{(-1)^m}{\eta_{ij}^{d_{ij}} (d_{ij}-1)! m!} \int_0^{+\infty} \mathrm{e}^{-\left(1+\frac{1}{\eta_{ij}}\right) r} r^{i+k-1} dr \\ &= \sum_{m=0}^{k_r} (-1)^m \binom{k_r}{m} \binom{m+d_{ij}-1}{m} \frac{\eta_{ij}^m}{(1+\eta_{ij})^{m+d_{ij}}} \qquad (12) \end{aligned}$$

The Erlang distribution suffers from some drawbacks. The parameter d_{ij} is equal to the ratio between the square mean value and the variance of the distribution. Hence, when modelling a distribution with constant variance and arbitrary large mean value, the value of d_{ij} may significantly increase with potential numeric inaccuracy.

C. Biased Rayleigh distribution for Pairwise Distance

The *biased Rayleigh* distribution is an alternative model we adopt to model the distribution of pairwise distances. The PDF of biased Rayleigh for $r \geqslant 0$ is

$$p_{r_{ij}}(r) = \frac{1}{\mathrm{K}_{br_{ij}}} \, r \, \exp\left(-\frac{(r-\mu_{ij})^2}{2\sigma_{ij}^2} \right) \tag{13}$$

where $\mu_{ij} \geqslant 0$ is the mode and $\sigma_{ij} > 0$ is the width. The mode and the width are parameters setting the shape of the distributions and must not be confused with the mean value and the standard deviation. If $\mu_{ij} = 0$, then eq. (13) becomes the PDF of standard Rayleigh distribution. The *unnormalized moment* of order m is defined as

$$\begin{aligned} \mathcal{M}_m(\mu, \sigma) &= \int_0^{+\infty} t^{m+1} \, \mathrm{e}^{-\frac{(t-\mu)^2}{2\sigma^2}} \, dt \\ &= \begin{cases} \sigma \sqrt{\frac{\pi}{2}} \left(1 + \mathrm{erf}\left(\frac{\mu}{\sigma\sqrt{2}} \right) \right) & \text{if } m = -1 \\ \sigma\mu\sqrt{\frac{\pi}{2}} \left(1 + \mathrm{erf}\left(\frac{\mu}{\sigma\sqrt{2}} \right) \right) + \sigma^2 \mathrm{e}^{-\frac{\mu^2}{2\sigma^2}} & \text{if } m = 0 \\ \mu \, \mathcal{M}_{m-1}(\mu, \sigma) + m \, \sigma^2 \, \mathcal{M}_{m-2}(\mu, \sigma) & \text{otherwise} \end{cases} \end{aligned} \tag{14}$$

The value of unnormalized moment is given above in the form of recurrent definition. The moments can be used to find the normalization constant $\mathrm{K}_{br_{ij}}$, the mean value $\mu_{br_{ij}}$ and the variance $\sigma_{br_{ij}}^2$ as

$$\mathrm{K}_{br_{ij}} = \mathcal{M}_0(\mu_{ij}, \sigma_{ij}) \quad \mu_{br_{ij}} = \frac{\mathcal{M}_1(\mu_{ij}, \sigma_{ij})}{\mathcal{M}_0(\mu_{ij}, \sigma_{ij})} \tag{15}$$

$$\sigma_{br_{ij}}^2 = \frac{\mathcal{M}_2(\mu_{ij}, \sigma_{ij})}{\mathcal{M}_0(\mu_{ij}, \sigma_{ij})} - \left(\frac{\mathcal{M}_1(\mu_{ij}, \sigma_{ij})}{\mathcal{M}_0(\mu_{ij}, \sigma_{ij})} \right)^2 \tag{16}$$

The biased Rayleigh PDF can be expanded into a series of Laguerre polynomials as shown in eq. (9). The coefficients $c_{k_r}^{ij}$ for this expansion are

This article has been accepted for publication in a future issue of this journal, but has not been fully edited. Content may change prior to final publication. Citation information: DOI 10.1109/LRA.2019.2891432, IEEE Robotics and Automation Letters

$$
\begin{aligned}
c_{k_r}^{ij} &= \int_0^{+\infty} \mathrm{e}^{-r} \, \frac{1}{\mathrm{K}_{br_{ij}}} \, r \, \exp\left(-\frac{(r-\mu_{ij})^2}{2\sigma_{ij}^2}\right) L_j(k_r) dr \\
&= \sum_{m=0}^{k_r} \binom{n}{m} \frac{(-1)^{k_r} \mathrm{e}^{\mu_{ij} - \frac{\sigma_{ij}^2}{2}}}{\mathrm{K}_{br_{ij}} \; m!} \int_0^{+\infty} \mathrm{e}^{-\frac{(r-(\mu_{ij}-\sigma_{ij}^2))^2}{2\sigma_{ij}^2}} r^{m+1} dr \\
&= \sum_{m=0}^{k_r} \binom{n}{m} \frac{(-1)^{k_r} \mathrm{e}^{\mu_{ij} - \frac{\sigma_{ij}^2}{2}}}{\mathrm{K}_{br_{ij}} \; m!} \, \mathcal{M}_m(\mu_{ij} - \sigma_{ij}^2, \sigma_{ij})
\end{aligned} \tag{17}
$$

D. Signature Distribution of Point Sets

There are all the elements to derive an efficient approximation of the signature distribution in eq. (2). The series approximation is based on the approximation of marginals of eq. (5) and (9). The two series are arrested respectively to order n_θ for random variable θ and n_r for random variable r. Thus, the signature distribution is approximated by $p_{\theta r}(\theta, r) \simeq \mathcal{S}(\theta, r)$ defined as

$$
\begin{aligned}
\mathcal{S}(\theta, r) &= \frac{1}{N} \sum_{i=1}^{n_p} \sum_{j=i+1}^{n_p} \left(\sum_{k_r=0}^{n_r} c_{k_r}^{ij} \; L_{k_r}(r) \right) \\
&\quad \cdot \left(\sum_{k_\theta=0}^{n_\theta} \left(a_{k_\theta}^{ij} \cos(k_\theta \theta) + b_{k_\theta}^{ij} \sin(k_\theta \theta) \right) \right) \\
&= \sum_{k_\theta=0}^{n_\theta} \sum_{k_r=0}^{n_r} \omega_{k_\theta k_r}(\theta, r)
\end{aligned} \tag{18}
$$

where the terms $\omega_{k_\theta k_r}(\cdot)$ and their parameters are equal to

$$
\begin{aligned}
&\omega_{k_\theta k_r}(\theta, r) = A_{k_\theta k_r} L_{k_r}(r) \cos(k_\theta \theta) + B_{k_\theta k_r} L_{k_r}(r) \sin(k_\theta \theta) \\
&A_{k_\theta k_r} = \sum_{i=1}^{n_p} \sum_{j=i+1}^{n_p} \frac{a_{k_\theta}^{ij} c_{k_r}^{ij}}{N} \quad B_{k_\theta k_r} = \sum_{i=1}^{n_p} \sum_{j=i+1}^{n_p} \frac{b_{k_\theta}^{ij} c_{k_r}^{ij}}{N}
\end{aligned} \tag{19}
$$

The coefficients $c_{k_r}^{ij}$ in the above equations refer to the Erlang or biased Rayleigh depending on the chosen model. The novel form of eq. (18) has the advantage of having a fixed form independently from the number of point pairs N. The complexity of signature computation lies in the coefficients of the above series. The basis functions $L_{k_r}(r)\cos(k_\theta\theta)$ and $L_{k_r}(r)\sin(k_\theta\theta)$ are orthogonal. This makes the signature suitable for analytical manipulation as illustrated in the following section. Figure 2 represents the two GRD signatures obtained using respectively biased Rayleigh and Erlang distributions to represent range uncertainty. The signature obtained by Erlang is smoother and less detailed than the one by biased Rayleigh. In general, it is more difficult to shape Erlang kernel PDF according to the desired variance due to discretization and numerical issues of integer exponent d_{ij} in eq. (13).

IV. A Metric for Signature Distributions

Signature distribution represents the geometric relations of a local map of points. The main goal of signatures is detection of already visited places or, at least, of potential candidate matches. A rotation-invariant metric should be used to compare a given target distribution signature $\mathcal{S}_t$ with a potential

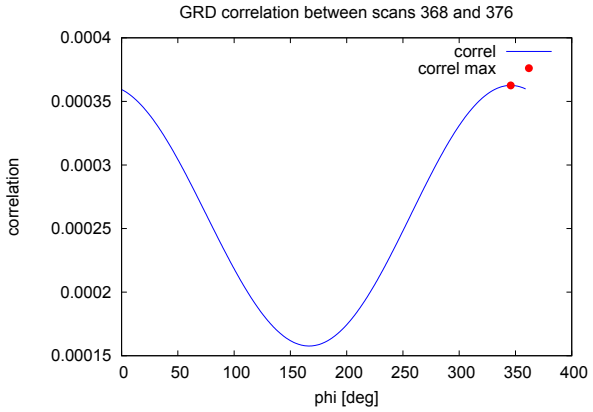

Fig. 3: Example of GRD signature correlation between the scans 368 and 376 of dataset *intel*. Maximum correlation is achieved with angular shift $\varphi = 345.8\ deg$ (equivalent to $-14.2\ deg$) consistent with point rotation (see Figure 1).

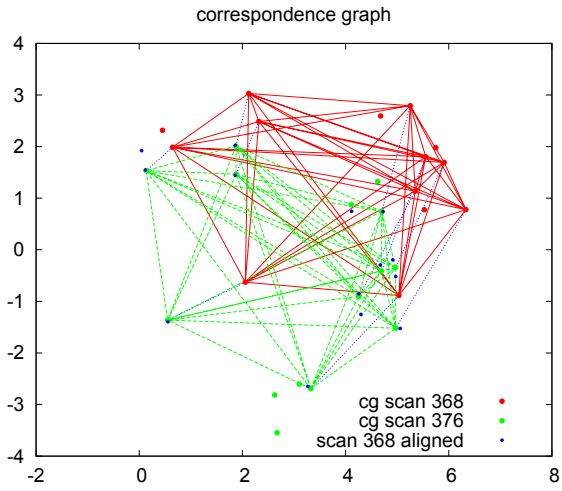

Fig. 4: Example of point-to-point association using correspondence graph (CG): the keypoint features of scans 368 (red) and 376 (green) in Figure 1 with their pairwise relation graphs, and the features 368 aligned to features 376 (blue).

matching one $\mathcal{S}_s$. While the pairwise distances are invariant to translation and rotation, the pairwise angles depend on the viewpoint. To achieve invariance, we follow the criterion adopted for GLAROT [4]. The similarity between the signature distributions $\mathcal{S}_t$ and $\mathcal{S}_s$ (apices or pedices s and t are used hereafter) is defined as

$$
d(\mathcal{S}_s, \mathcal{S}_t) = \max_{\varphi} \frac{d_\varphi(\mathcal{S}_s, \mathcal{S}_t)}{\sqrt{d_0(\mathcal{S}_s, \mathcal{S}_s) \; d_0(\mathcal{S}_t, \mathcal{S}_t)}} \tag{20}
$$

where

$$
d_\varphi(\mathcal{S}_s, \mathcal{S}_t) = \int_0^{2\pi} d\theta \int_0^{\infty} dr \; \mathrm{e}^{-r} \; \mathcal{S}_s(\theta + \varphi, r) \; \mathcal{S}_t(\theta, r) \tag{21}
$$

Instead of being a distance, the quantity $d(\cdot)$ is maximum when the two distributions represent the geometric relations of the

This article has been accepted for publication in a future issue of this journal, but has not been fully edited. Content may change prior to final publication. Citation information: DOI 10.1109/LRA.2019.2891432, IEEE Robotics and Automation Letters

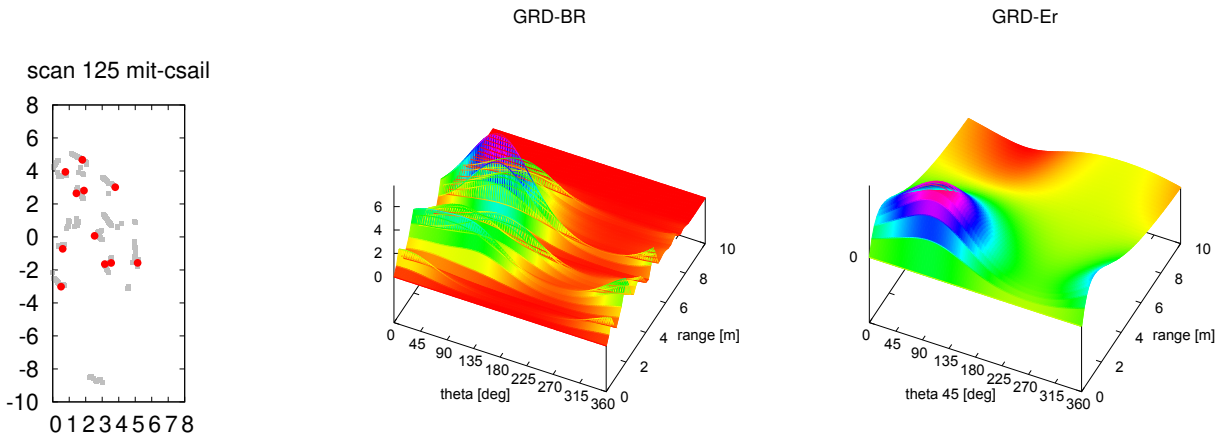

(a) (b) (c)

Fig. 2: Example of GRD signatures computed on a mit-csail dataset: (a) the input scan (grey) with the extracted FLIRT features (red); (b) the GRD-BR signature obtained using biased Rayleigh distribution for ranges (with parameters $(\kappa, \sigma_{ij}) = (1.5, 0.2)$); (c) the GRD-Er signature obtained using Erlang distribution for ranges (with parameters $(\kappa, \sigma_{ij}) = (1.5, 0.2)$). The GRD-Er signature is smoother than GRD-BR one and provides less details.

same point set. The integral in eq. (20), which consists of a product of two truncated series, could be difficult to solve. Let $\omega^s_{k_\theta k_r}(\cdot)$ and $\omega^t_{k_\theta k_r}(\cdot)$ be the terms of series $\mathcal{S}_s$ and $\mathcal{S}_t$ according to eq. (18), with coefficients respectively $\{A^s_{k_\theta k_r}, B^s_{k_\theta k_r}\}$ and $\{A^t_{k_\theta k_r}, B^t_{k_\theta k_r}\}$. The integral of $\omega^s_{k_\theta k_r}(\cdot)\omega^t_{k'_\theta k'_r}(\cdot)$ is zero if $k_\theta \neq k'_\theta$ or $k_r \neq k'_r$ due to the orthogonality of the basis function. Thus, the only remaining terms are $\omega^s_{k_\theta k_r}(\cdot)\omega^t_{k_\theta k_r}(\cdot)$. In particular, the integral is solved as

$$\begin{aligned}\zeta_{k_\theta k_r}(\varphi) &= \int_0^{2\pi}\int_0^{\infty} \mathrm{e}^{-r}\omega^s_{k_\theta k_r}(\theta+\varphi, r)\omega^t_{k_\theta k_r}(\theta, r)d\theta dr \\ &= \frac{A^s_{k_\theta k_r}A^t_{k_\theta k_r} + B^s_{k_\theta k_r}B^t_{k_\theta k_r}}{2}\cos(k_\theta\varphi) \\ &\quad + \frac{A^s_{k_\theta k_r}B^t_{k_\theta k_r} - B^s_{k_\theta k_r}A^t_{k_\theta k_r}}{2}\sin(k_\theta\varphi) \end{aligned} \tag{22}$$

After the substitution of eq. (22) in the metric expression, we obtain

$$d_\varphi(\mathcal{S}_s, \mathcal{S}_t) = \sum_{k_\theta=0}^{n_\theta}\sum_{k_r=0}^{n_r}\zeta_{k_\theta k_r}(\varphi) \tag{23}$$

$$= \sum_{k_\theta=0}^{n_\theta} A^\varphi_{k_\theta k_r}\cos(k_\theta\varphi) + B^\varphi_{k_\theta k_r}\sin(k_\theta\varphi) \tag{24}$$

where the coefficients $\{A^\varphi_{k_\theta k_r}, B^\varphi_{k_\theta k_r}\}$ are obtained as

$$A^\varphi_{k_\theta k_r} = \sum_{k_r=0}^{n_r}\frac{A^s_{k_\theta k_r}A^t_{k_\theta k_r} + B^s_{k_\theta k_r}B^t_{k_\theta k_r}}{2} \tag{25}$$

$$B^\varphi_{k_\theta k_r} = \sum_{k_r=0}^{n_r}\frac{A^s_{k_\theta k_r}B^t_{k_\theta k_r} - B^s_{k_\theta k_r}A^t_{k_\theta k_r}}{2} \tag{26}$$

Figure 3 shows the correlation function $d_\varphi(\mathcal{S}_s, \mathcal{S}_t)$ for the keypoint features presented in Figure 1. It can be observed that the harmonic component $k_\theta = 1$ dominates over higher frequency components. The estimated angular shift φ, where d_φ is maximum, provides a rather accurate estimation of rotation angle between the two feature maps.

Signatures are used for retrieval of candidates matching local maps. Next the candidates are checked by performing point-to-point association. The *Correspondence Graph* (CG) [4] searches potential correspondences based on the same pairwise geometric relations used by GRD signature. Since CG exploits the consistency of matching points, it does not rely on the estimation of local map reference frames w.r.t. the global reference frame. Figure 4 shows the CG association for the previously discussed example.

V. Experiments

In this section we present our experimental setup and results based on loop closure. The experiments are assessed in four public datasets: *fr079*, *mit-csail*, *intel-lab* and *fr-clinic*. The datasets provided by [6] contain both original scans and corresponding corrected ground truth. Results are presented with precision-recall curves for loop closure tests.

The loop closure experiments are evaluated comparing each scan $\mathcal{S}_i$ with the other scans of the dataset $\mathcal{S}_j$ with $j \neq i$. The proposed loop closure algorithm GRD[1], both with Erlang (GRD-Er) and biased Rayleigh (GRD-BR), has been tested in each dataset and compared with two state-of-the-art algorithms, GFP and GLAROT. We evaluate the original GFP algorithm using FLIRT keypoints and descriptors, since signature GFP was originally coupled with the specific keypoint feature. The keypoint features SKIP [22] are used to build the landmark maps encoded by GLAROT and GRD. Signature evaluation requires that loop closure candidates are tested with point-to-point association. GFP uses RANSAC algorithm as point-to-point association method according to its original formulation and implementation. The other signatures are evaluated with point-to-point matching method *Correspondence Graph* (CG) [4].

[1] https://github.com/dlr1516/grd.

This article has been accepted for publication in a future issue of this journal, but has not been fully edited. Content may change prior to final publication. Citation information: DOI 10.1109/LRA.2019.2891432, IEEE Robotics and Automation Letters

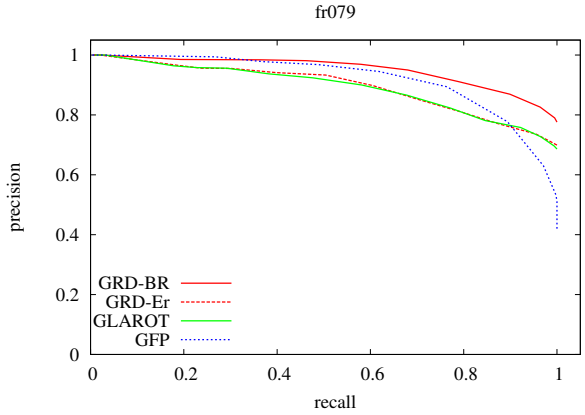

Fig. 5: Precision-recall curves of loop closure based on GRD-BR, GRD-Er, GLAROT and GFP in datasets *fr079*.

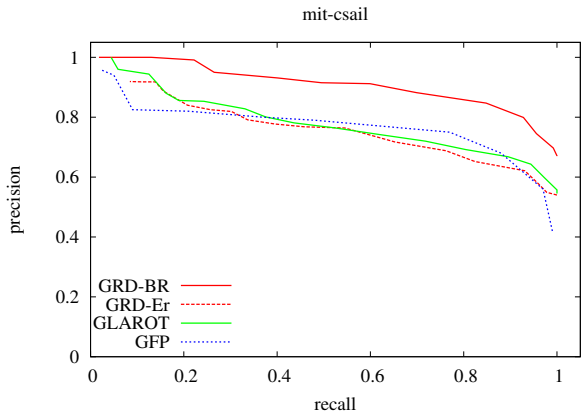

Fig. 6: Precision-recall curves of loop closure based on GRD-BR, GRD-Er, GLAROT and GFP in datasets *mit-csail*.

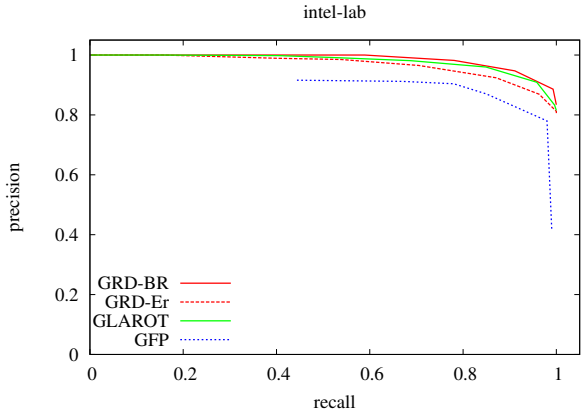

Fig. 7: Precision-recall curves of loop closure based on GRD-BR, GRD-Er, GLAROT and GFP in datasets *intel-lab*.

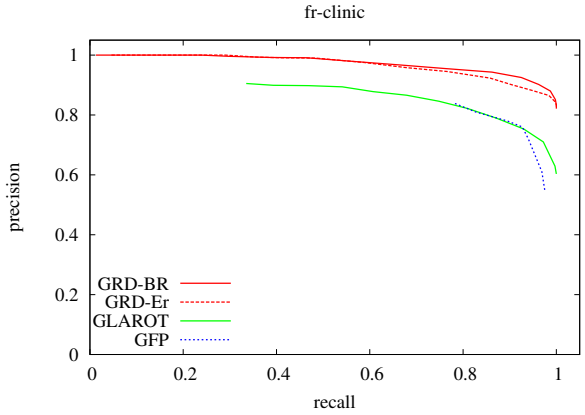

Fig. 8: Precision-recall curves of loop closure based on GRD-BR, GRD-Er, GLAROT and GFP in datasets *fr-clinic*.

The loop closure evaluation has been performed as follows. For each scan $\mathcal{S}$ of a dataset the scan signatures have been computed and stored. Then, let $\mathcal{S}_R$ be the reference scan, a set $\mathcal{C}_S$ of 20 candidate scans (50 for GFP), whose signatures are closest to the signatures of the reference scan $\mathcal{S}_R$ according to the respective loop closure method, are extracted. The set of closest signatures $\mathcal{C}_S$ is evaluated according to the corresponding distance function and thresholds of each loop closure method. The keypoints of each scan in $\mathcal{C}_S$ are associated with $\mathcal{S}_R$ using the selected point-to-point association algorithm. Then, the robot pose is estimated by solving the orthogonal Procrustes problem on associated point pairs. Finally, the scan selected for loop closure $\bar{\mathcal{S}}_i$ is the scan that, after alignment, has the greatest number of keypoints with a neighbor point in $\mathcal{S}_R$ within the $0.10\ m$ range. The place recognition performance is measured by precision-recall curves. The robot is considered localized if the associated points are at least N_{min}. The precision-recall curves are computed w.r.t. the threshold N_{min}. A localization is considered correct when the position error of the aligned scan is less than $0.50\ m$ and the angular error less than $10°$.

Figures 5-8 depict the precision-recall curves obtained in datasets *fr079*, *intel*, *mit-csail* and *fr-clinic* with the place recognition algorithms previously discussed. GFP achieves results comparable to the other features in dataset *fr079*, but in the other cases it is dominated by the other approaches. Its performance may be affected by the use of FLIRT features and descriptors used in the local map. Previous works [3], [4] have already observed the potential weakness of local descriptors for LIDAR measurements and the arising limitation of the resulting BoW detection. The curves of GLAROT, GRD-BR and GRD-Er tend to overlap in the case *intel*, but GRD-BR dominates GLAROT all the other approaches. While all such signatures are based on geometric relations, GRD-BR seems to provide a more accurate representation of cumulated pairwise distances and angles.

Indeed, GLAROT discretizes these parameters into histogram bins whereas GRD-Er exploits Erlang distribution, which achieves smoother and less detailed description than biased Rayleigh, as shown in Figure 2. Thus, the proposed GRD signature is able to select potential loop closure candidates with similar or better performance compared to other state-of-the-art methods like GLAROT.

The efficiency of the signatures has been empirically assessed by signature matching with datasets *fr079*, *intel*, *mit-*

operation		avg time [μs]
GFP	construction	2722.0
	pairwise distance	3.7
GLAROT	construction	138.7
	pairwise distance	4.2
GRD-Er	construction	2052.4
	pairwise distance	275.2
GRD-BR	construction	2445.0
	pairwise distance	274.6
CG association		538.6
SKIP detection		97.5

TABLE I: Average times per scan required for creation and pairwise distance of signatures (GFP, GLAROT, GRD-Er and GRD-BR) and for CG point-to-point association. The times have been computed on datasets *fr079*, *intel*, *mit-csail* and *fr-clinic* with an average number of 13.47 detected features per scan.

csail and *fr-clinic*. The execution times presented in Table I are obtained on an Intel i7-3630QM CPU @ 2.40GHz, 8 GB RAM processor. In particular, these tests measure the average execution time for the construction of signatures and for the computation of single pairwise distance between two signatures. A single loop closure query requires the computation of the pairwise distances between the query signature and all the other signatures of the map. The construction time for GRD signatures is about one order of magnitude greater than GLAROT, but comparable with GFP whose complexity is due to the initial offline computation with BoW dictionary. The complexity of GRD construction is quadratic with the number of point features whereas the pairwise distance computation is computed using guaranteed branch-and-bound optimization with $1\ deg$ tolerance on correlation (compared with $22.5\ deg$ bin size of GLAROT). Moreover, the computation time could be significantly improved by an optimized implementation and better parameter tuning.

VI. Conclusion

In this paper, we have presented the novel signature GRD for landmark map location in order to recognize visited places for localization and loop closure. The signature corresponds to the probability density function of the pairwise angles and distances among the landmarks of a local map. The distribution models for the two polar coordinates are respectively von Mises for angles and Erlang or biased Rayleigh for distances. The signature GRD has been expanded into series of orthogonal function basis, namely Fourier series and Laguerre polynomials. The coefficients of the series have been derived and used to represent the signature. This representation enables efficient analytic operations with multimodal distribution and, in particular, allows the definition of rotation and translation invariant metric to compare the distribution. The GRD capability to detect visited places in the map has been compared with other state-of-the-art signatures in loop closure experiments.

In future works, we expect to apply GRD in the loop closure component of a localization and mapping system. Moreover, we will investigate the extension of GRD signature to 3D landmark maps and the design of scale-invariant metrics suitable for computer vision applications.

References

[1] G. D. Tipaldi, L. Spinello, and K. O. Arras, "Geometrical flirt phrases for large scale place recognition in 2d range data," in *Proc. of the IEEE Int. Conf. on Robotics & Automation (ICRA)*, 2013, pp. 2693–2698.

[2] M. Himstedt, J. Frost, S. Hellbach, H.-J. Boehme, and E. Maehle, "Large scale place recognition in 2D lidar scans using geometrical landmark relations," in *Proc. of the IEEE/RSJ Int. Conf. on Intelligent Robots and Systems (IROS)*, 2014, pp. 5030–5035.

[3] F. Kallasi, D. Lodi Rizzini, and S. Caselli, "Fast keypoint features from laser scanner for robot localization and mapping," *IEEE Robotics and Automation Letters (RA-L)*, vol. 1, no. 1, pp. 176–183, jan 2016, dOI 10.1109/LRA.2016.2517210.

[4] F. Kallasi and D. Lodi Rizzini, "Efficient Loop Closure based on FALKO LIDAR Features for Online Robot Localization and Mapping," in *Proc. of the IEEE/RSJ Int. Conf. on Intelligent Robots and Systems (IROS)*, 2016, pp. 1206–1213.

[5] J. Deray, J. Solà, and J. Andrade-Cetto, "Word ordering and document adjacency for large loop closure detection in 2-d laser maps," *IEEE Robotics and Automation Letters (RA-L)*, vol. 2, no. 3, pp. 1532–1539, 2017.

[6] G. D. Tipaldi and K. O. Arras, "Flirt-interest regions for 2d range data," in *Proc. of the IEEE Int. Conf. on Robotics & Automation (ICRA)*, 2010, pp. 3616–3622.

[7] J.-S. Gutmann and K. Konolige, "Incremental Mapping of Large Cyclic Environments," in *Proc. of the IEEE Int. Symposium on Computational Intelligence in Robotics and Automation (CIRA)*, 1999, pp. 318–325.

[8] M. Himstedt and E. Maehle, "Geometry matters: Place recognition in 2D range scans using Geometrical Surface Relations," in *Proc. of the European Conference on Mobile Robots (ECMR)*, 2015, pp. 1–6.

[9] T. Bailey, E. Nebot, J. Rosenblatt, and H. Durrant-Whyte, "Data association for mobile robot navigation: a graph theoretic approach," in *Proc. of the IEEE Int. Conf. on Robotics & Automation (ICRA)*, 2000, pp. 2512–2517.

[10] P. San Segundo and D. Rodriguez-Losada, "Robust global feature based data association with a sparse bit optimized maximum clique algorithm," vol. 29, no. 5, pp. 1332–1339, Oct 2013.

[11] J. Neira and J. Tardós, "Data Association in Stochastic Mapping Using the Joint Compatibility Test," *IEEE Trans. on Robotics*, vol. 17, no. 6, pp. 890–897, 2001.

[12] F. Lu and E. Milios, "Globally Consistent Range Scan Alignment for Environment Mapping," *Journal of Autonomous Robots*, vol. 4, pp. 333–349, 1997.

[13] E. Mendes, P. Koch, and S. Lacroix, "ICP-based pose-graph SLAM," in *IEEE Int. Sym. on Safety, Security, and Rescue Robotics (SSRR)*, 2016, pp. 195–200.

[14] W. Hess, D. Kohler, H. Rapp, and D. Andor, "Real-Time Loop Closure in 2D LIDAR SLAM," in *Proc. of the IEEE Int. Conf. on Robotics & Automation (ICRA)*, 2016, pp. 1271–1278.

[15] D. Lodi Rizzini, "Place Recognition of 3D Landmarks based on Geometric Relations," in *Proc. of the IEEE/RSJ Int. Conf. on Intelligent Robots and Systems (IROS)*, 2017, pp. 648–654.

[16] Y. Tazaki, Y. Miyauchi, and Y. Yokokohji, "Loop detection of outdoor environment using proximity points of 3d pointcloud," in *2017 IEEE/SICE International Symposium on System Integration (SII)*, Dec 2017, pp. 411–416.

[17] G. Kim and A. Kim, "Scan context: Egocentric spatial descriptor for place recognition within 3d point cloud map," in *In Proceedings of the IEEE/RSJ International Conference on Intelligent Robots and Systems*, 2018.

[18] J. Aleotti, D. Lodi Rizzini, R. Monica, and S. Caselli, "Global Registration of Mid-Range 3D Observations and Short Range Next Best Views," in *Proc. of the IEEE/RSJ Int. Conf. on Intelligent Robots and Systems (IROS)*, 2014, pp. 3668–3675.

[19] M. Abramowitz and I. Stegun, *Handbook of Mathematical Functions*. Dover Publications, 1965.

[20] D. Lodi Rizzini, "Angular Radon Spectrum for Rotation Estimation," *Pattern Recognition*, vol. 84, pp. 182–196, dec 2018.

[21] N. Lebedev, *Special Functions and Their Applications*. Englewood Cliffs, N.J.: Prentice-Hall Inc., 1965.

[22] D. Lodi Rizzini, F. Galasso, and S. Caselli, "Safe Feature-based Navigation for Industrial AGVs," in *Proc. of IROS Workshop on Robotics for logistics in warehouses and environments shared with humans*, 2018.